1 Title of thesis

Micro-watt energy harvesting by exploiting the flow around a circular cylinder-strip plate cruciform

2 Project outline

This work seeks to exploit the flow-induced vibration (FIV) due to vortex shedding around a circular cylinder–strip plate cruciform to generate power. The circular cylinder is elastically mounted, and the periodic shedding of the vortices create the alternate lift that drives the vibration of the cylinder.

In a pure cruciform configuration between the cylinder and plate, i.e. both aretilted $\pi/2$ rad to each other, a vibration response is elicited from the elastically mounted cylinder that exceeds the maximum vibration amplitude of an isolated cylinder, under similar flow conditions. This is desirable from an energy harvesting perspective since a higher vibration amplitude translates into higher harnessable energy from the fluid stream.

What sets off the high amplitude vibration in the cruciform setup? What is the limit for improvement for the amplitude response? How can we generalise the cruciform setup as a method for flow and vibration control? These are the questions that we seek to answer in this study.

3 Data collection

We studied the questions raised in §2 through the use of numerical methods to solve the continuity and Navier-Stokes equations around the problem geometery previously defined. We opted for the open source C++ library OpenFOAM due to its portability in case file management (the whole case are just text files placed in a directory tree that obeys a simple convention) and extensibility in terms of the solution of the governing equations, dynamic mesh handling and workflow customisation and automation (which is possible simply by using shell scripts or by using Python, through PyFOAM).

We collect field data such as velocity, pressure and vorticity from the numerical results to visually grasp key points in the temporal evolution of the fluid-structure interaction between the cruciform and the stream. This lays the qualitative base to our description and understanding of the flow field. We also collect one-dimensional time series data of the lift coefficient and also mean turbulent velocity fluctuations at certain locations downstream the cylinder for quantitive analysis of the vibration response.

To generalise the cruciform setup of circular cylinder-strip plate as a method for vibration response control, we varied the tilt angle of the plate, relative to the axis of the cylinder, in from 0 rad to $\pi/2$ rad in increments of $\pi/8$ rad. This allows us to gauge how sensitive the vortical structures driving the vibration are with respect to structural symmetry.

4 Data analysis

4.1 Methods of analysis

The one-dimensional time series data, which is oscillatory in nature, are analysed for their root-mean-square amplitude values and dominant frequency content to reveal amplitude and frequency response of the system with respect to the reduced velocity U^*. The dominant frequency of the

system, is generally determined via fast Fourier transform (FFT) for the cylinder displacement time series (or "signal" for short). The root-mean-square (RMS) amplitude for the lift signal however, is computed after the signal is decomposed using ensemble empirical mode decomposition (EEMD) (Huang et al. 1998; Wu and Huang 2008), and its prevalent frequency, after computing the Hilbert spectrogram of the decomposed lift signal. We discuss why in the following paragraph.

In our past leg of study which focussed on the $\pi/2$ rad case, we observed that the lift signal behaves less sinusoidal with the advent of streamwise vortex and streamwise vortex-induced vibration (SVIV). In fact, following EEMD, we identified two components of that decomposition (also known as intrinsic mode functions or IMF) with the highest RMS amplitude, and computed their Hilbert spectrograms. What results is the discovery that these two IMFs–two with the largest RMS amplitudes–oscillate at a mean frequency close to the shedding frequency of Karman vortex (or simply the Karman frequency) while the other, oscillates close to the natural frequency of the system. Our choice of using EEMD to compute the Hilbert spectrogram allows us to gain a better understanding not only of the principal constituents of lift signal frequency, but also its temporal evolution and more generally, the degree of dispersion of the instantaneous frequencies from the mean.

4.2 Generalising the pure cruciform configuration

Figure 1 summarises the amplitude responses of the cylinder with varying U^* and θ_{plate}. We chose to study the effect of θ_{plate} variation in addition to U^* because variation of θ_{plate} is one of the most straightforward ways to generalise the $\pi/2$ rad case which is a pure cruciform configuration. The $\pi/2$ rad case is now just one of the infinite cruciform possibilities in which the plate is tilted from 0 rad to $\pi/2$ rad. This not only is the first attempt to grasp the sensitivity of the system to cruciform symmetry, but is also potentially a method to control the contribution of the streamwise and Karman vortices towards the total lift amplitude.

At $\theta_{\text{plate}} = 0$ rad, the amplitude response shows a tremendously different trend compared to the reference case of $\theta_{\text{plate}} = \pi/2$ rad: the root-mean-square value of the normalised cylinder displacement y^*_{RMS} starts its growth from a very low U^* of 9.1, monotonically increases up to $U^* = 18.2$, before saturating close to $y^*_{\text{RMS}} \approx 0.8$ at that U^*. We hypothesize that this form of amplitude response is the result of the strengthening of streamwise vorticity across the spanwise direction of the cylinder. Where previously the streamwise vorticity is amplified into a sustainable flow structure only in the vicinity of the strip plate, the 0 rad plate destabilises the streamwise vorticity along the length of the cylinder, thus bringing into realisation multiple streamwise vortices simultaneously. This brings the transition to streamwise vortex-dominant regime down to $U^* = 9.1$ and imposes a larger lift on the cylinder compared to the $\pi/2$ rad case. We remind the reader that although not at $\pi/2$ rad, the plate at 0 rad is definitely a symmetrical configuration. This symmetry is broken once we rotate the plate by $\pi/8$ rad, which we discuss next.

At $\theta_{\text{plate}} = \pi/8$ rad, the symmetry of the cylinder-plate configuration is broken. This pushes the start of the vibration regime up to a higher $U^* = 20.5$. This is an indication that the shear layer instabilities along the cylinder must be stronger compared to when $\theta_{\text{plate}} = 0$ rad, for the now asymmetrical strip plate to have an effect on the amplification and sustenance of the streamwise vorticity, which is responsible for the high-amplitude response from the cylinder. We also observe that even at the same U^*, the root-mean-square amplitude of vibration is smaller for the case of $\pi/8$ rad as can be seen from the y^*_{RMS} values $U^* = 20.5$ through 29.5. $U^* = 20.5$. This suggest that the lift produced by the vortices at this θ_{plate} is smaller at $\pi/8$ rad, in contrast to when $\theta_{\text{plate}} = 0$ rad. Inspecting Fig. 2 reveals some evidence that supports this hypothesis.

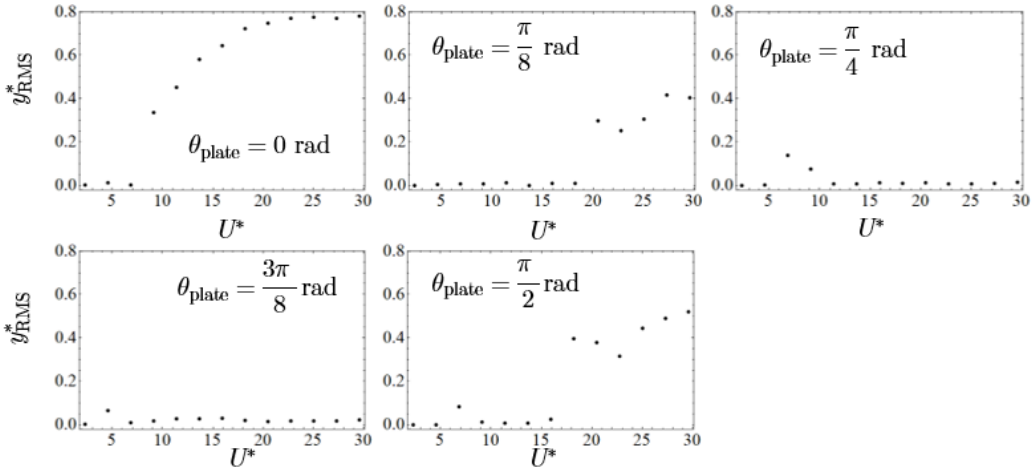

Figure 1: Amplitude response for various values of θ_{plate} from $0 \leq \theta_{\mathrm{plate}}$ (rad) $\leq \pi/2$.

Specifically, Fig. 2 summarises how the root-mean-square of the cylinder lift force varies with respect to U^*. The sudden jump in $F_{\mathrm{L,RMS}}$ at $U^* = 20.5$ results in a similar jump in y^*_{RMS}, as can be seen in Fig. 1. This correlation is of course expected, as dicussed in Raghavan (2007) and Bernitsas et al. (2008).

As we increase the tilt further to $\pi/4$ rad, we observe that the highest amplitude response is now well below $U^* = 20.5$, which is at $U^* = 6.8$ (see Fig. 1). Incidentally, the value of 6.8 at where the maximum y^*_{RMS} exists is uncannily close to the typical U^* where the upper branch exists for the high-mass ratio, low-damping case of an isolated circular cylinder. This hints that while the typical amplitude response of an isolated cylinder is suppressed at θ_{plate} 0 rad and $\pi/8$ rad, the system manages to recover this trend as θ_{plate} reaches $3\pi/8$ rad. The reason behind this is probably because at this θ_{plate}, the amount of interference provided by the plate is the furthest away from the two poles of symmetry–$\theta_{\mathrm{plate}} = 0$ rad and $\pi/2$ rad. The interference imposed by the plate at $\theta_{\mathrm{plate}} = \pi/4$ rad is concentrated mid-length of the cylinder, which is similar to the $\theta_{\mathrm{plate}} = \pi/2$ rad case. However, this interference introduced mid-lenth of the cylinder is aymmetrical, which as a consequence retards any meaningful interaction between the shear layers near the cylinder-plate juncture. Of course, this explanation is only coherent if the examination of a θ_{plate} closer to $\pi/2$ rad yields an amplitude response closer to the response of a pure cruciform system ($\theta_{\mathrm{plate}} = \pi/2$ rad). We discuss about this next.

When we increase the tilt further to $\theta_{\mathrm{plate}} = 3\pi/8$ rad, we observe the amplitude response peaks at $U^* = 4.5$. Similar to the $\pi/4$ rad case, $U^* = 4.5$ is close to the U^* where the KVIV upper branch exists. Consequently, we find it reasonable to attribute this peak to Karman vortex shedding. Despite this peak most probably is the manifestation of the KVIV upper branch, similar to the peak when $\theta_{\mathrm{plate}} = \pi/4$ rad, the magnitude of this peak is comparatively smaller to the peak at $\pi/4$ rad. The suppression of KVIV is one of the anticipated effects of a pure cruciform system i.e., $\theta_{\mathrm{plate}} = \pi/2$ rad (Shirakashi, Mizuguchi, and Bae 1989). Reminded of this fact, it is highly probable that the downsizing of the peak amplitude at $3\pi/8$ rad results from the same mechanism that suppresses KVIV in a pure cruciform system. It thus follows that this takes place because $\theta_{\mathrm{plate}} = 3\pi/8$ rad is closer to $\pi/2$ rad, compared to $\pi/4$ rad. Even

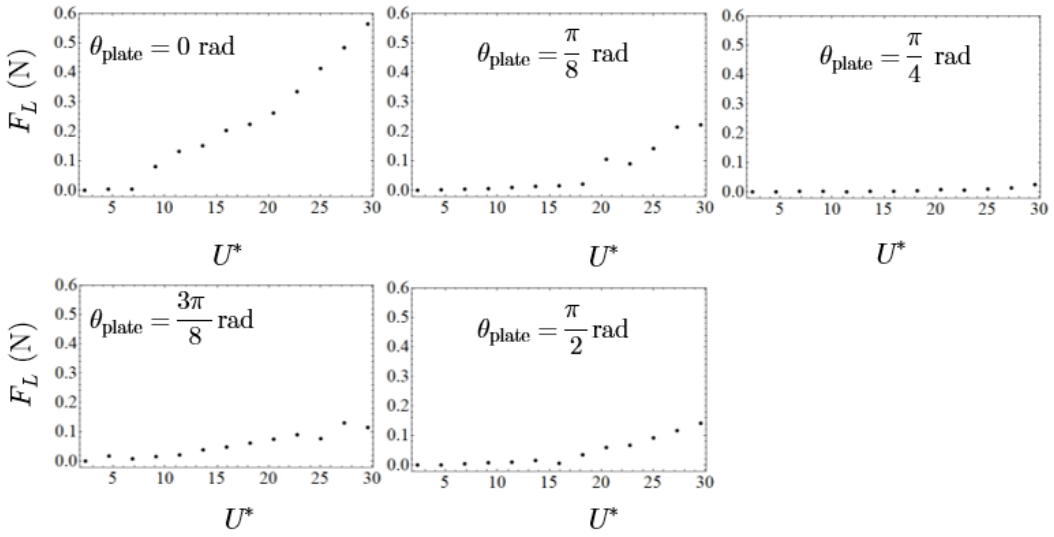

Figure 2: Lift force variation with respect to U^* and θ_{plate}.

though $\theta_{\text{plate}} = 3\pi/8$ rad is closer to $\pi/2$ rad compared to $\pi/4$ rad, the value of $3\pi/8$ rad may just be insufficient for streamwise vortex pairs to form and be strong enough to drive cylinder vibration after the desynchronisation region of KVIV.

This result suggests two things. First, it shows that the degree of symmetry is paramount to obtain coherent vortical structures that is responsible for the creation of a well-behaved alternating lift on the cylinder. As the tilt of the plate approaches one of the poles of symmetry, i.e. θ_{plate} = 0 rad or $\pi/2$ rad, the vortical structures resulting from the fluid-structure interaction become their most coherent version of themselves. Deviating from either poles of symmetry introduces a degree of asymmetry which the instabilities are sensitive to, arresting the coherence and strength of the prime vortices, thus decreasing the alternating lift amplitude and consequently y^*_{RMS}.

Second, there seems to be a difference in the level of sensitivity of the vortical structures towards the asymmetry introduced as θ_{plate} is varied between $0 < \theta_{\text{plate}}$ (rad) $< \pi/2$. For example, the amplitude response of $\theta_{\text{plate}} = 0$ rad and $\pi/8$ rad. One can simply inspect Fig. 1 to see how the high-amplitude response of the cylinder remains present, only shifted to a higher U^* and at a much lower magnitude of y^*_{RMS}. But the high-amplitude response regime still exist, and seems to exist over a much larger range of U^* compared to the isolated cylinder case (Koide et al. 2009). This does not seem to be the case for the vortical structure when $\theta_{\text{plate}} = \pi/2$ rad. The vortical structure at $\theta_{\text{plate}} = \pi/2$ rad seems to be more sensitive to the asymmetry of the configuration introduced when θ_{plate} is $3\pi/8$ rad. As a result, the similarity between the amplitude responses at $\theta_{\text{plate}} = 3\pi/8$ rad and $\pi/2$ rad ends at the reduction of the peak amplitude at U^* close to 5. The onset of the high-amplitude vibrations that occurs at U^* = 18.2 is not observed when $\theta_{\text{plate}} = 3\pi/8$ rad.

These discussions point to the possibility of using the tilt of the plate as a valid way to control the type of amplitude response we get from the cruciform system, and its magnitude. It is tempting to correlate the amplitude response in Fig. 1 as being one-dimensionally dependent of the amplitude of lift, whose root-mean-square values are summarised in Fig. 2. However, one

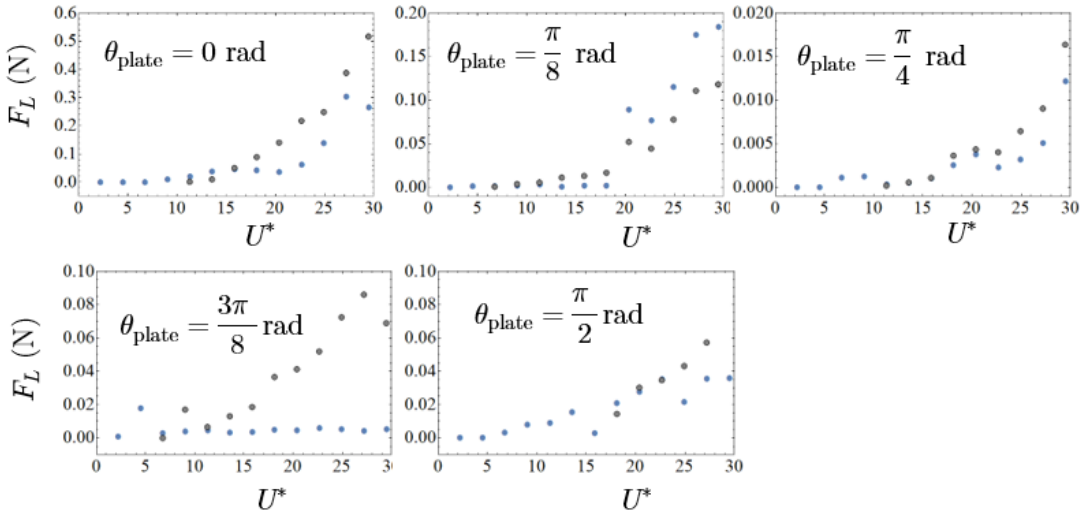

Figure 3: The evolution of the two most dominant components of lift after its decomposition using EEMD, against U^* and θ_{plate}.

quickly finds that for certain cases, the RMS amplitude of lift does not have a positive correlation with y^*_{RMS}, e.g. between cases $\theta_{\text{plate}} = \pi/4$ rad, $3\pi/8$ rad, and $\pi/2$ rad.

4.3 Dominant components of the lift signal

When we compare the amplitude response for $\theta_{\text{plate}} = \pi/4$ rad and $3\pi/8$ rad, it is clear that the magnitude for y^*_{RMS} when $U^* > 11.4$ are very similar. This observation seems to be at odds with the $F_{\text{L,RMS}}$ evolution shown in Fig. 2, or its enlarged version in Fig. 3. This is because while $F_{\text{L,RMS}}$ when $\theta_{\text{plate}} = 3\pi/8$ rad is unambiguously bigger than the $F_{\text{L,RMS}}$ when $\theta_{\text{plate}} = \pi/4$ rad (in the region $11.4 \leq U^* \leq 29.5$), the magnitude of y^*_{RMS} are very similar to each other. Why is this the case?

To answer this question, we decomposed the lift signal using EEMD producing a number of IMFs for each lift signal processed. Then, we look for the IMF component with the highest correlation to the displacement signal at the same θ_{plate} and U^*. Looking for the IMF component with the highest correlation to the displacement signal $y(t)$ results in singling out the component of lift that is most similar to the $y(t)$ in terms of temporal evolution of amplitude and frequency, differing only in phase. What we found out in our previous investigation of the $\theta_{\text{plate}} = \pi/2$ rad case reveals that this component of lift, which is most similar to $y(t)$ in terms of amplitude and frequency distribution may not be the component with the largest RMS amplitude among the other IMFs from the same IMF set.

For the case of $\theta_{\text{plate}} = \pi/2$ rad, another IMF component of RMS amplitude comparable to, or larger than, the component most similar to the displacement signal (hereafter designated as $C_{F_L,y(t)}$) appears in the IMF set once U^* reaches the onset of SVIV. This new component, although its RMS amplitude is similar to, or larger than $C_{F_L,y(t)}$, its mean instantaneous frequency

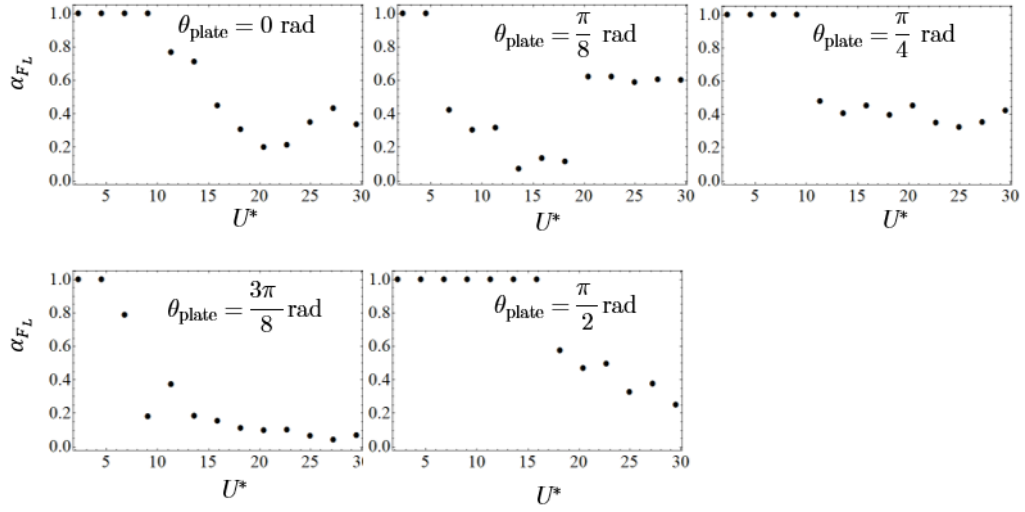

Figure 4: The evolution of the ratio between two dominant components of the lift signal with respect to U^* and θ_{plate}.

is not. Its mean instantaneous frequency is generally fairly close to the frequency of Karman vortex shedding from a smooth, isolated circular cylinder. Indeed this is the case for tilt angles $\theta_{\text{plate}} = 0$ rad, $\pi/8$ rad, $3\pi/8$ rad, and $\pi/2$ rad. The only case where the IMF component with the largest RMS amplitude has a mean frequency that does not follow the Karman frequency pattern is the case of $\theta_{\text{plate}} = \pi/4$ rad. Instead, the IMF component with the largest RMS amplitude (hereafter denoted as $C_{F_L,\max}$) keeps its mean instantaneous frequency close to 16 Hz, throughout for all U^* studied.

Once we are aware of the existence of two dominant components of the lift signal at certain velocities, we can understand why the amplitude response of $\theta_{\text{plate}} = \pi/4$ rad and $3\pi/8$ rad are similar above $U^* = 11.4$, even though $F_{\text{L,RMS}}$ at these same velocities are markedly larger for the case of $3\pi/8$ rad. If we look at Fig. 3, we can easily see that although the RMS amplitude of the total lift is larger for the case of $\theta_{\text{plate}} = 3\pi/8$ rad compare to $\theta_{\text{plate}} = \pi/4$ rad, the actual component of lift that is close to the natural frequency of the system is only approximately 20% of the total RMS amplitude of lift, as summarised in Fig. 4. Furthermore, in terms of magnitude, the RMS amplitude of $C_{F_L,y(t)}$ is only as large as the $C_{F_L,y(t)}$ at $\theta_{\text{plate}} = \pi/4$ rad. So it is not surprising when the y^*_{RMS} of both $\theta_{\text{plate}} = \pi/4$ rad and $3\pi/8$ rad in the range $11.4 < U^* < 29.5$ are of similar magnitude.

The discrepancy between the magnitude of $F_{\text{L,RMS}}$ for $\theta_{\text{plate}} = 3\pi/8$ rad and $\pi/2$ rad can also be explained in a similar fashion: although the magnitudes for $F_{\text{L,RMS}}$ are similar at $\theta_{\text{plate}} = 3\pi/8$ rad and $\pi/2$ rad (see Fig. 2), the RMS amplitude of $C_{F_L,y(t)}$ is higher when $\theta_{\text{plate}} = \pi/2$ rad, compared to when $\theta_{\text{plate}} = 3\pi/8$ rad. This therefore producing a higher value of y^*_{RMS} for the cylinder displacement.

As we have demonstrated earlier, sometimes understanding Figs. 1 and 2 requires the aid of Fig. 4. Therefore we have summarised the evolution of α_{F_L} against U^* for all θ_{plate} studied.

As previously mentioned, the quantity α_{F_L} in Fig. 4 is computed by selecting the component of IMF with the highest correlation to the displacement signal. Whenever the component with the highest correlation to the displacement signal $C_{F_L,y(t)}$ also happens to be the component with the highest RMS amplitude, it is given a value of 1, denoting 100%. However, when $C_{F_L,y(t)}$ is not simultaneously the component with the highest RMS amplitude $C_{F_L,\max}$, we determine which of the other IMF components–with a lower correlation to the displacement signal–is the $C_{F_L,\max}$ for the given U^* and θ_{plate}. Then, we compute the ratio α_{F_L} as follows.

$$\alpha_{F_L} = \frac{C_{F_L,y(t)}}{C_{F_L,y(t)} + C_{F_L,\max}} \tag{1}$$

We would like to make it clear however, that Eq. 1 is not aimed to quantify the RMS amplitude of the component of lift driving the cylinder vibration as a fraction of the total RMS amplitude of lift, but rather as an index to compare the contribution to $F_{\text{L,RMS}}$ by the principal components of lift. In doing so, it will be easier to estimate the percentage of harnessable power lost to the most energetic flow structures, whose cycle of formation and decay fail to lock into the natural frequency of the system f_n.

5 Chapters completed and progress to date

6 Factors impeding the progress of research

References

Bernitsas, Michael M.M. et al. (Nov. 2008). "VIVACE (Vortex Induced Vibration Aquatic Clean Energy): A New Concept in Generation of Clean and Renewable Energy From Fluid Flow". In: *Journal of Offshore Mechanics and Arctic Engineering* 130.4, p. 041101. ISSN: 08927219. DOI: 10.1115/1.2957913. URL: http://www.scopus.com/record/display.url?eid=2-s2.0-56749179917%7B%5C&%7Dorigin=resultslist%7B%5C&%7Dsort=plf-f%7B%5C&%7Dsrc=s%7B%5C&%7Dst1=A+new+concept+in+generation+of+clean+and+renewable+energy+from+fluid+flow%7B%5C&%7Dsid=620865A71FAF26768C42655E1E8BC194.aXczxbyuHHiXgaIW6Ho7g:230%7B%5C&%7Dsot=b%7B%5C&%7Dsdt=b%7B%5C&%7D%20h.

Huang, Norden E. et al. (1998). "The empirical mode decomposition and the Hubert spectrum for nonlinear and non-stationary time series analysis". In: *Proceedings of the Royal Society A: Mathematical, Physical and Engineering Sciences*. ISSN: 13645021. DOI: 10.1098/rspa.1998.0193.

Koide, Mizuyasu et al. (2009). "A Novel Technique for Hydroelectricity Utilizing Vortex Induced Vibration". In: *Proceedings of the ASME Pressure Vessels and Piping Division Conference, PVP2009-77487*.

Raghavan, Kamaldev (2007). "Energy Extraction from a Steady Flow Using Vortex Induced Vibration." English. Doctoral Dissertation. The University of Michigan, pp. 1–344. URL: http://deepblue.lib.umich.edu/handle/2027.42/55687.

Shirakashi, M., K. Mizuguchi, and H. M. Bae (1989). "Flow-induced excitation of an elastically-supported cylinder caused by another located downstream in cruciform arrangement". In: *Journal of Fluids and Structures* 3.6, pp. 595–607. ISSN: 10958622. DOI: 10.1016/S0889-9746(89)90150-3.

Wu, Zhaohua and Norden E. Huang (2008). "Ensemble Empirical Mode Decomposition: A Noise-Assisted Data Analysis Method". In: *Advances In Adaptive Data Analysis*. ISSN: 1793-5369. DOI: 10.1142/S1793536909000047.